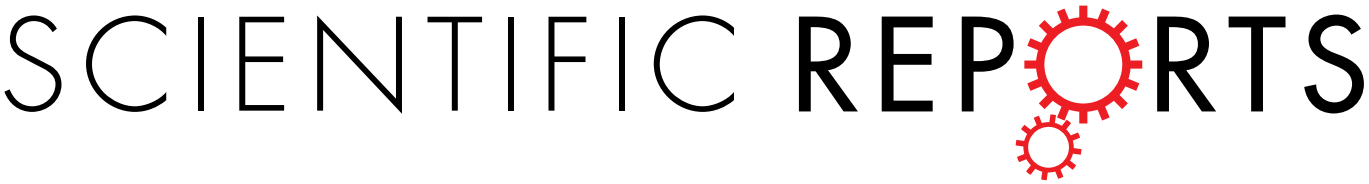

OPEN

In-plane Isotropic Microwave Performance of CoZr Trilayer in GHz Range

Received: 14 October 2015
Accepted: 21 January 2016
Published: 17 February 2016

Lulu Pan, Fenglong Wang, Wenfeng Wang, Guozhi Chai & Desheng Xue

In this paper, we investigate the high frequency performance of $Co_{90}Zr_{10}/SiO_2/Co_{90}Zr_{10}$ trilayers. It is demonstrated that the in-plane isotropic microwave performance is theoretically derived from the solution of the Landau-Lifshitz-Gilbert equation and experimentally achieved in that sandwich structured film. The valuable isotropic behavior comes from the superposition of two uncouple ferromagnetic layers in which the uniaxial magnetic anisotropic fields are equivalent but mutually orthogonal. Moreover, the isotropic microwave performance can be tuned to higher resonance frequency up to 5.3 GHz by employing the oblique deposition technique. It offers a convenient and effective way to achieve an unusual in-plane isotropic microwave performance with high permeability in GHz, holding promising applications for the magnetic devices in the high frequency information technology.

Soft magnetic materials with isotropic high permeability (IHP) at working frequency are crucial components in modern information technology because of their extensive applications to improve the performance of magnetic devices such as micro-transformers, planar inductors and core materials of writing head[1–3]. Nowadays, data transfer rate is getting to GHz, but the classical Snoek's law[4] indicates that the IHP based on crystalline anisotropy in the traditional microwave soft magnetic materials can only be obtained in the MHz range. To find the desired materials with IHP in the GHz range is still a challenge. For instance, a variety of theoretical[5–7] and experimental works focus on both high[8–10] and isotropic[11–18] permeability in the GHz range of granular films[9] and multilayers[10] of magnetic alloys, ferrites and their composites.

As Kittel predicted in 1947[19], magnetic thin film is a good candidate to achieve high permeability in the GHz range. The high permeability in the GHz range was measured experimentally in the CoZrNb magnetic thin films with an in-plane uniaxial magnetic anisotropy (IPUMA) in 1996[20]. Subsequently, many film systems of alloys, ferrites and their composites have been investigated[8,9,21–23]. Therein, metallic magnetic thin films, which have higher saturation magnetization than ferrite films, are better to achieve higher permeability and resonance frequency. Besides the large saturation magnetization M_s, the large IPUMA is essential for high permeability in the GHz range[24]. As the frequency response of the permeability is almost flat up to a rolloff frequency, associated with ferromagnetic resonance, when a microwave magnetic field $\mathbf{h}$ is applied perpendicular to the IPUMA field $\mathbf{H}_K$, the resonance frequency f_r and initial permeability μ_{in} of the magnetic thin films can be adjusted by H_K as $f_r = (\gamma/2\pi)\sqrt{(M_s + H_K)H_K}$[19] with γ as the gyromagnetic ratio and $\mu_{in} = M_s/H_K$[22], respectively. In fact, the IPUMA field $\mathbf{H}_K$ has been modulated by many effective methods, such as composition gradient sputtering[25,26], micro-stripe patterning[27–30], annealing under magnetic fields[31–33], inducing stress on substrates[34–36], oblique deposition[37,38], temperature[39] and electric field control[40,41], etc. The permeability higher than 100 was achieved in the 1–5 GHz range in (Fe, Co)-based magnetic thin films with the IPUMA[24]. However, the high permeability of magnetic thin films with the IPUMA is anisotropic, which depends on the relative direction of $\mathbf{h}$ with respect to $\mathbf{H}_K$.

Searching for the isotropic permeability in the GHz range is another important topic in magnetic thin films. For instance, magnetic thin films with rotatable stripe domain[42–46], composite-anisotropy multilayer as well as crossed anisotropies multilayer[11–18] are intensively investigated. The rotatable stripe domain was discovered firstly in Permalloy films in 1961[42], and then in many other magnetic thin films[43–46]. As the effective IPUMA is along the direction of the stripe domain, the in-plane omnidirectional equivalent permeability can be achieved[46] by rotating the stripe domain. It is worth noting that this is a spurious isotropic performance, because an external

Key Laboratory for Magnetism and Magnetic Materials of the Ministry of Education Lanzhou University, Lanzhou, 730000, People's Republic of China. Correspondence and requests for materials should be addressed to G.C. (email: chaigzh@lzu.edu.cn) or D.X. (email: xueds@lzu.edu.cn)

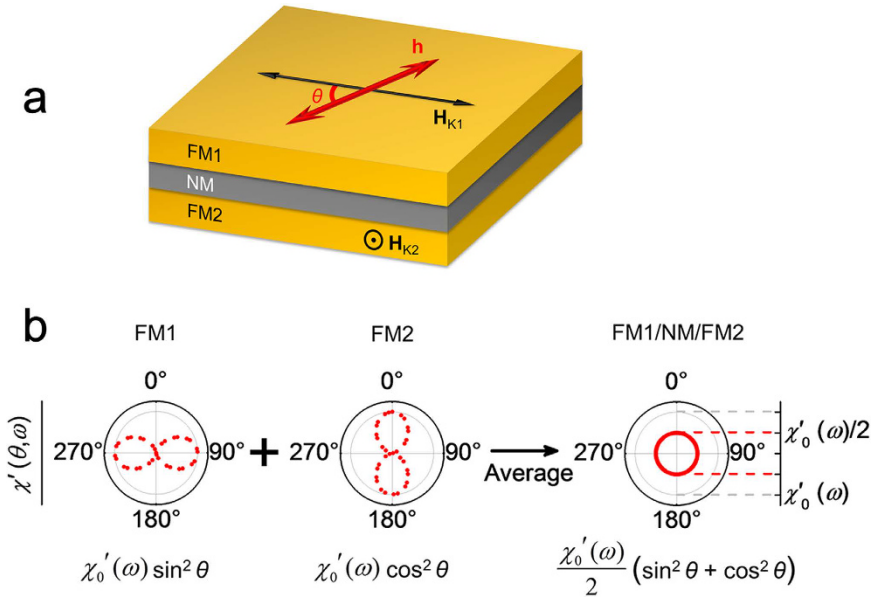

Figure 1. Schematic diagram and the angular dependences of the susceptibility of FM1/NM/FM2 film. (**a**) $\mathbf{H}_{K1}$ and $\mathbf{H}_{K2}$ ($\mathbf{H}_{K1} \perp \mathbf{H}_{K2}$, and $H_{K1} = H_{K2}$) are the in-plane uniaxial magnetic anisotropy fields of the FM1 and FM2 ferromagnetic layers, NM is the non-ferromagnetic interlayer, and θ is the angle between $\mathbf{H}_{K1}$ and the microwave magnetic field **h**. (**b**) θ dependences of the susceptibility under **h**, where the left, middle and right polar diagrams are theoretical simulation results of FM1, FM2 and FM1/NM/FM2, respectively.

saturated magnetic field needs to be applied to rotate the orientation of the stripe domains which may limit the application of the magnetic thin films in magnetic devices. Similar results are found in other magnetic thin films with rotatable anisotropy[46]. The composite-anisotropy multilayer[11–15] is another idea to search for the isotropic permeability, in which many equivalent magnetic layers having the same IPUMA are piled up. Similar to a random particle composite, the overall anisotropy of the multilayer can be cancelled out by shifting sequentially the anisotropic axis of every layer from bottom to surface[11]. The isotropic permeability is then achieved. Furthermore, the crossed anisotropies multilayers[16–18] were also investigated for the purpose of isotropic permeability. However, the resonance frequencies of those multilayers are normally lower than 2 GHz. Therefore, seeking for magnetic thin films with the IHP in higher frequency is still expected not only for fundamental research but also for the technological applications.

In this paper, we report the achievement of an in-plane IHP with resonance frequency higher than 5 GHz in a convenient FM1/NM/FM2 (FNF) film, in which two ferromagnetic layers (FMi, $i = 1, 2$) are decoupled by a non-ferromagnetic interlayer (NM). By theoretical analysis, FM1 and FM2 with the same magnetic moment and equivalent but mutually orthogonal IPUMA fields H_K are proposed. The isotropic microwave performance with an in-plane IHP is found experimentally in a $Co_{90}Zr_{10}/SiO_2/Co_{90}Zr_{10}$ FNF film. Moreover, it is indicated that the in-plane IHP characteristics of these FNF films can even be extended to higher working frequency by employing the oblique deposition technique.

Theoretical analysis

Figure 1 illustrates the FNF film designed to realize the in-plane IHP in the GHz range, in which the IPUMA fields are perpendicular to each other. Considering a microwave magnetic field **h** applied in the plane of the FNF film as shown in Fig. 1a, the complex susceptibility of the film comes from weighted average of complex susceptibility of FM1 and FM2, written as

$$\chi'(\omega, \theta) = \sum_{i=1}^{2} p_i \chi'_i, \tag{1}$$

$$\chi''(\omega, \theta) = \sum_{i=1}^{2} p_i \chi''_i, \tag{2}$$

where p_i ($i = 1, 2$) is the volume ratio of the FMi layer to the two magnetic layers. The microwave susceptibility of each magnetic layer results from uniform precession of magnetization, which can be described by LLG equation[47], so the susceptibility of FMi layer (χ'_i and χ''_i) can be derived from LLG equation, and given by

$$\chi'_i(\omega, \theta) = \frac{(\gamma M_{si})^2 [\gamma^2 M_{si} H_{Ki} - \omega^2]}{[\gamma^2 M_{si} H_{Ki} - \omega^2]^2 + \omega^2 \alpha_i^2 \gamma^2 M_{si}^2} \sin^2\left[(i-1)\frac{\pi}{2} - \theta\right], \tag{3}$$

$$\chi''_i(\omega, \theta) = \frac{(\gamma M_{si})^3 \omega\alpha_i + \gamma M_{si}\omega^3\alpha_i}{[\gamma^2 M_{si}H_{Ki} - \omega^2]^2 + \omega^2{\alpha_i}^2\gamma^2 M_{si}^2} \sin^2\left[(i-1)\frac{\pi}{2} - \theta\right], \tag{4}$$

where γ is the gyromagnetic ratio, α_i is damping parameter, ω is the angular frequency of $\mathbf{h}$ and θ is the angle between $\mathbf{h}$ and $\mathbf{H}_{K1}$, respectively. As $\mu' = 1 + \chi'(\omega, \theta)$ and $\mu'' = \chi''(\omega, \theta)$, the complex permeability is generally angular dependent. Combining Equation (1), (2), and Equation (3), (4) with the conditions of

$$M_{s1} = M_{s2} = M_s \quad \text{and} \quad p_1 = p_2 = 1/2, \tag{5}$$

$$\mathbf{H}_{K1} \perp \mathbf{H}_{K2} \quad \text{and} \quad H_{K1} = H_{K2} = H_K, \tag{6}$$

$$\alpha_1 = \alpha_2 = \alpha, \tag{7}$$

an angular independent complex permeability of the FNF film can be derived as

$$\mu'(\omega) = 1 + \frac{1}{2}\chi'_0(\omega), \tag{8}$$

$$\mu''(\omega) = \frac{1}{2}\chi''_0(\omega). \tag{9}$$

Herein, χ'_0 and χ''_0 are the real and imaginary parts of the complex susceptibility of a single FM layer under the condition $\mathbf{h} \perp \mathbf{H}_K$, as[48]

$$\chi'_0(\omega) = \frac{(\gamma M_s)^2[\gamma^2 M_s H_K - \omega^2]}{[\gamma^2 M_s H_K - \omega^2]^2 + \omega^2\alpha^2\gamma^2 M_s^2}, \tag{10}$$

$$\chi''_0(\omega) = \frac{(\gamma M_s)^3\omega\alpha + \gamma M_s\omega^3\alpha}{[\gamma^2 M_s H_K - \omega^2]^2 + \omega^2\alpha^2\gamma^2 M_s^2}. \tag{11}$$

Consequently, the in-plane IHP can be realized in the FNF film as shown in Fig. 1(b).

Results and Discussion

In experiments, $Co_{90}Zr_{10}$(100 nm)/SiO_2(10 nm)/$Co_{90}Zr_{10}$(100 nm) FNF films with in-plane IHP at GHz were fabricated by radio-frequency magnetron oblique sputtering (see Supplementary Fig. S1 online). Here $Co_{90}Zr_{10}$ (EDS and XRD data are shown in Supplementary Fig. S2 online) used as FM layer, which possesses a relative high saturation magnetization and a well-established IPUMA[49,50], can result in the high permeability at GHz. Each $Co_{90}Zr_{10}$ layer was about 100 nm to ensure that $M_{s1} = M_{s2} = M_s$ and $p_1 = p_2 = 1/2$. A 10 nm SiO_2 interlayer was chosen to eliminate the exchange coupling between two FMs, and thus the IPUMA of each $Co_{90}Zr_{10}$ layer can be adjusted separately. The direction and strength of the IPUMA were induced by controlling the oblique deposition conditions to satisfy $\mathbf{H}_{K1} \perp \mathbf{H}_{K2}$ and $H_{K1} = H_{K2}$, $\alpha_1 = \alpha_2 = \alpha$ as the two $Co_{90}Zr_{10}$ layers are equivalent. The details are discussed in the supplementary information.

Static magnetic performance. Figure 2 depicts the in-plane magnetic hysteresis loops of the $Co_{90}Zr_{10}$ FNF film fabricated by 30° oblique deposition, as well as that of a $Co_{90}Zr_{10}$(100 nm) single layer as a comparison. Two significant characteristics of the loops shown in Fig. 2a indicate that the conditions for achieving IHP are met in the $Co_{90}Zr_{10}$ FNF film. Shape of the loops in Fig. 2a, which is different from that in Fig. 2b, can be explained as the superposition of loops along the easy and hard axis of FM, respectively. The loops parallel and perpendicular to the direction of $\mathbf{H}_{K1}$ are almost identical, which implies the saturation magnetization, as well as the anisotropies, of FM1 and FM2 are equivalent, i.e., $M_{s1} = M_{s2}$ and $H_{K1} = H_{K2}$. To clarify the results above, the remanence and the slope near $H = 0$ Oe are discussed further in the following. The remanence ratio of 0.53 shown in Fig. 2a is the weighted average of the remanence ratios 0.99 and 0.05 obtained from the easy and hard axis loops in Fig. 2b, that means $\mathbf{H}_{K1} \perp \mathbf{H}_{K2}$. Moreover, the equal remanence M_{ri} ($i = 1, 2$) $\approx M_{si}/2$ along $\mathbf{H}_{Ki}$, indicates $M_{s1} = M_{s2}$. Meanwhile, the same slope at $H = 0$ Oe for both loops, which can be expressed as M_s/H_K, reveals $H_{K1} = H_{K2}$ as well. As the $Co_{90}Zr_{10}$ FNF film satisfies the conditions for achieving IHP very well, it is expected to have in-plane IHP as predicted by Equation (8)–(11). It should be noted that the hysteresis loops of FNF trilayer are not fully isotropic even the permeability of the FNF is angular independent.

Dynamic magnetic performance. The microwave performances of the $Co_{90}Zr_{10}$ FNF film and a $Co_{90}Zr_{10}$ single layer are shown in Fig. 3. Figure 3(a,b) displays a typical frequency dependence of the real (imaginary) part of the sample permeability μ' (μ'') measured at $\theta = 90°$. The real part μ' higher than 50 is obtained from 1.0 to 2.5 GHz. The fitting results indicate both the $Co_{90}Zr_{10}$ FNF film and the single layer exhibit a resonance-type permeability spectra, i.e. the spectrum of the real (imaginary) part is a dispersive (Lorentzian) curve. In order to demonstrate the isotropic microwave properties, the angular dependence of the resonance frequency, the maximum value and the full width at half maximum (FWHM) of the imaginary parts are plotted in Fig. 3c–e, respectively. The angular independence of the three characteristic quantities of the Lorentzian curves indicates

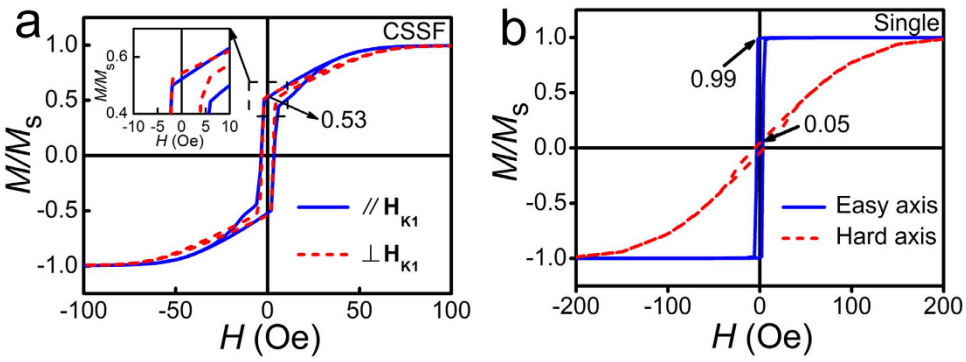

Figure 2. In-plane magnetic hysteresis loops of the films fabricated by 30° oblique deposition. (**a**) Loops of the $Co_{90}Zr_{10}/SiO_2/Co_{90}Zr_{10}$ FNF film. The blue solid line and red dashed line represent the curves measured along and perpendicular to the anisotropy field $\mathbf{H}_{K1}$. The insert is an enlarged view of the loops near the remnant ratio 0.53. (**b**) Loops of the $Co_{90}Zr_{10}$ single layer. The blue solid line and red dashed line represent the curves measured along easy and hard axis, in which the remnant ratios are 0.99 and 0.05, respectively.

that the imaginary part of the $Co_{90}Zr_{10}$ FNF film is isotropic. Based on the Kramers-Kronig relation, the real part of the $Co_{90}Zr_{10}$ FNF film must be also isotropic, which is confirmed by the experimental data shown in Fig. 3f, where the angular dependence of the permeability μ' at 1 GHz of the $Co_{90}Zr_{10}$ FNF film shows clearly a circular characteristic of the IHP instead of a spindle-like distribution for the $Co_{90}Zr_{10}$ single layer. By fitting the data in Fig. 3f, the IHP at 1 GHz is around 55 for the $Co_{90}Zr_{10}$ FNF film. Those results reveal that the isotropic microwave performance with the IHP is achieved in the $Co_{90}Zr_{10}$ FNF film rather than in the $Co_{90}Zr_{10}$ single layer.

In order to extend experimentally the working frequency range of the $Co_{90}Zr_{10}$ FNF film with IHP and exploit the universality of the IHP of the FNF film, the $Co_{90}Zr_{10}$ FNF film with the same structure as previous but higher resonance frequency was fabricated by 40° oblique deposition. According to the self-shadow effect[51–53], the larger angle of the oblique deposition leads to the larger IPUMA field H_K of $Co_{90}Zr_{10}$ single layer and consequently the higher resonance frequency. The tunable high frequency properties of oblique deposited $Co_{90}Zr_{10}$ single layer can be found in Fig. S3 or in our previous works[49,50]. The isotropic microwave performances of this $Co_{90}Zr_{10}$ FNF film are displayed in Fig. 4, together with the corresponding data of 30° oblique deposition $Co_{90}Zr_{10}$ FNF film. Figure 4a shows typical frequency dependence of the real part of permeability for both $Co_{90}Zr_{10}$ FNF films. With the oblique deposition angle increasing from 30° to 40°, the f_r of the $Co_{90}Zr_{10}$ FNF film increases from 3.1 to 5.3 GHz. Figure 4b shows f_r vs θ plots, where the circular distribution implies the isotropic resonance frequency. The isotropic effective fields are calculated from the resonance frequency as about 299 Oe for $Co_{90}Zr_{10}$ FNF film fabricated by 40° oblique deposition and 102 Oe for the 30° oblique deposition sample. Figure 4c shows μ' at 1 GHz vs θ plots of the two $Co_{90}Zr_{10}$ FNF films as well as the fitted curves with Equation (8). The high frequency permeability always keep isotropic even the resonance frequency has been pushed from 3.1 to 5.3 GHz. These results reveal that the working frequency range of the $Co_{90}Zr_{10}$ FNF film with in-plane IHP can be adjusted by tuning the oblique deposition angle.

In conclusion, we have demonstrated that the $Co_{90}Zr_{10}$(100 nm)/SiO_2(10 nm)/$Co_{90}Zr_{10}$(100 nm) sandwich-structured films fabricated by the oblique deposition exhibit an isotropic microwave performance, and especially an isotropic high permeability larger than 20 with resonance frequency up to 5.3 GHz. The valuable isotropic behavior comes from the superposition of two uncouple equivalent ferromagnetic layers in which the uniaxial anisotropic fields are mutually orthogonal. The finding of the in-plane isotropic high permeability with high working frequency of the universal FM/NM/FM sandwich-structured film may benefit in searching for new microwave materials and have important applications in magnetic devices desired in the information technology.

Methods

Sample fabrication. The $Co_{90}Zr_{10}$(100 nm)/SiO_2(10 nm)/$Co_{90}Zr_{10}$(100 nm) sandwich-structured films and $Co_{90}Zr_{10}$(100 nm) single layer were deposited at room temperature onto Si (111) substrates by radio frequency magnetron sputtering, and the in-plane uniaxial magnetic anisotropy of each $Co_{90}Zr_{10}$ layer was induced by oblique deposition. The base vacuum is 8.5×10^{-5} Pa, the sputtering power is 50 W, the flow of Ar is 10 SCCM, and the sputtering pressure is 0.25 Pa. The component of $Co_{90}Zr_{10}$ layer is tuned by putting a few Zr chips on the Co target, and the thickness of each layer was controlled by deposition time and rate. The $Co_{90}Zr_{10}$ FNF film is deposited as follows: the $Co_{90}Zr_{10}$(100 nm) bottom layer on Si substrate is deposited firstly, after turning the sample by 90 degrees on the sample holder, SiO_2(10 nm) interlayer and the $Co_{90}Zr_{10}$(100 nm) top layer were deposited, successively.

Measurement. The composition of the films was determined by energy dispersive X-ray spectroscope (EDS) and the structure of the films was characterized by an X-ray diffractometer. A vibrating sample magnetometer (VSM) was employed to measure the hysteresis loops of the samples at room temperature. The remanence depending on angle of the $Co_{90}Zr_{10}$ FNF film was used to determine firstly the directions of $\mathbf{H}_{K1}$ and $\mathbf{H}_{K2}$, and then in-plane magnetic hysteresis loops were measured along $\mathbf{H}_{K1}$ and $\mathbf{H}_{K2}$. The similar measurement procedure was used for the $Co_{90}Zr_{10}$ single layer film as well. In order to get permeability spectra at different θ, we used

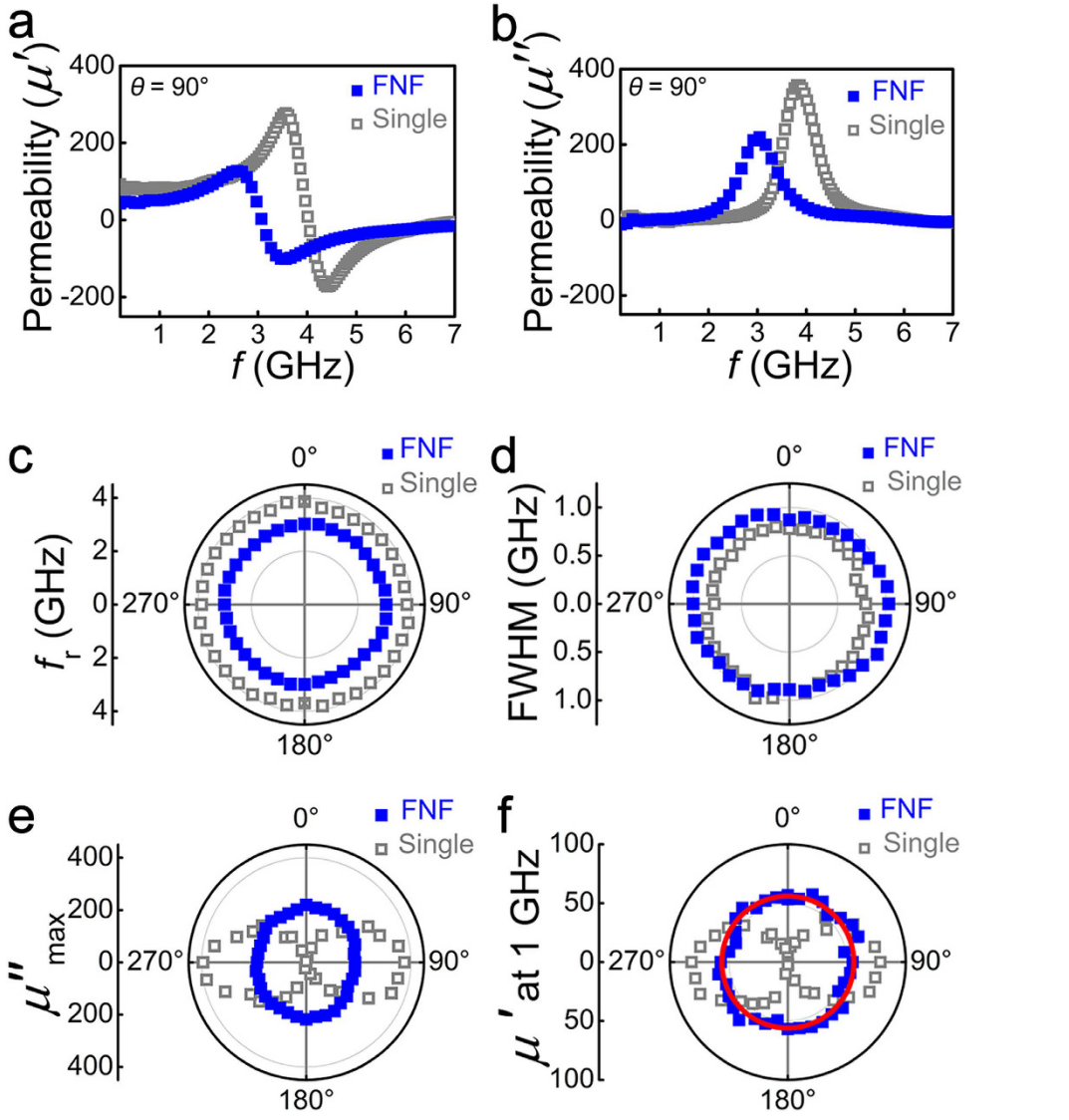

Figure 3. GHz frequency characteristics of the $Co_{90}Zr_{10}$ FNF film (blue solid squares) and the $Co_{90}Zr_{10}$ single layer (grey open squares) fabricated by 30° oblique deposition. (**a**) Real and (**b**) imaginary parts of permeability spectra measured at $\theta = 90°$. (**c**) Resonance frequency, (**d**) the FWHM, and (**e**) μ'' maximum as a function of θ. (**f**) Real part of permeability at 1 GHz as a function of θ. The red solid line is theoretical simulation result of $Co_{90}Zr_{10}$ FNF film.

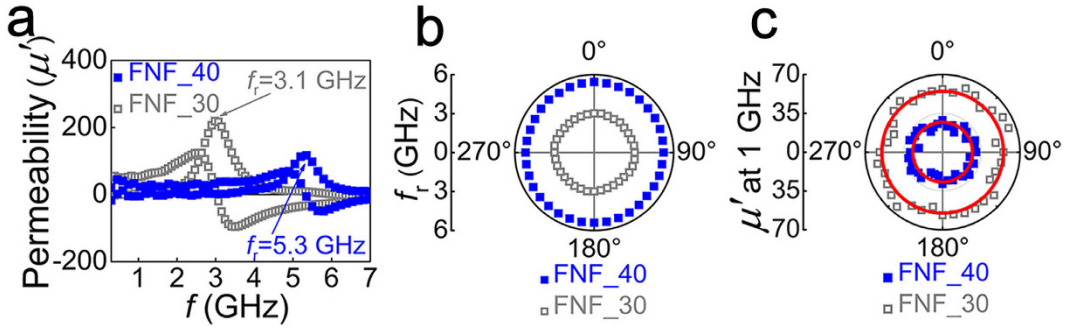

Figure 4. GHz frequency characteristics of the $Co_{90}Zr_{10}$ FNF films fabricated by 40° (blue solid squares) and 30° (grey open squares) oblique deposition. (**a**) permeability spectra. (**b**) θ dependence of resonance frequency f_r. (**c**) θ dependence of permeability (μ') at 1 GHz. The red solid lines are theoretical simulation results.

vector network analyzer (VNA) with shorted micro-strip method[54]. The isotropic effective field can be calculated from the resonance frequency with equation $f_r = (\gamma/2\pi)\sqrt{(M_s + H_K)H_K}$, but considering $H_K \ll M_s$ and for simplicity, $f_r = (\gamma/2\pi)\sqrt{M_s H_K}$ was used to calculate the effective field in this paper.

References

1. Osaka, T. *et al.* A soft magnetic CoNiFe film with high saturation magnetic flux density and low coercivity. *Nature* **392,** 796–798 (1998).
2. Wang, S. X., Sun, N. X., Yamaguchi, M. & Yabukami, S. Sandwich films: properties of a new soft magnetic material. *Nature* **407,** 150–151 (2000).
3. Parkin, S. *et al.* Magnetically engineered spintronic sensors and memory. *Proc. IEEE* **91,** 661–680 (2003).
4. Snoek, L. Dispersion and absorption in magnetic ferrites at frequencies above one Mc/s. *Physica* **14,** 207–217 (1948).
5. Perrin, G., Acher, O., Peuzin, J. C. & Vukadinovic, N. Sum rules for gyromagnetic permeability of ferromagnetic thin films: Theoretical and experimental results. *J. Magn. Magn. Mater.* **157-158,** 289–290 (1996).
6. Acher, O. & Adenot, A. L. Bounds on the dynamic properties of magnetic materials. *Phys. Rev. B* **62,** 11324–11327 (2000).
7. Acher, O. & Dubourg, S. Generalization of Snoek's law to ferromagnetic films and composites. *Phys. Rev. B* **77,** 104440 (2008).
8. Chai, G., Phuoc, N. N. & Ong, C. K. High thermal stability of zero-field ferromagnetic resonance above 5 GHz in ferrite-doped CoFe thin films. *Appl. Phys. Lett.* **103,** 042412 (2013).
9. Chai, G. *et al.* Magnetic properties of $(Co_{0.65}Fe_{0.35})_{1-x}(Ni_{0.5}Zn_{0.5}Fe_2O_4)_x$ bi-magnetic composite granular films for high frequency application. *J. Phys. D: Appl. Phys.* **42,** 205006 (2009).
10. Chai, G. *et al.* Adjust the resonance frequency of $(Co_{90}Nb_{10}/Ta)_n$ multilayers from 1.4 to 6.5 GHz by controlling the thickness of Ta interlayers. *Appl. Phys. Lett.* **96,** 012505 (2010).
11. Sugawara, E., Matsumoto, F., Fujimori, H. & Masumoto, T. Magnetic properties of composite anisotropy CoNbZr/Ceramics multilayers. *IEEE Trans. J. Magn. Jpn.* **7,** 969–974 (1992).
12. Cai, J. W., Kitakami, O. & Shimada, Y. Isotropic soft magnetic properties of CoFeAlCu films with (111) orientation. *J. Appl. Phys.* **79,** 1625–1629 (1996).
13. Shimada, Y., Sugawara, E. & Fujimori, H. Initial permeability of composite-anisotropy multilayer films. *J. Appl. Phys.* **76,** 2395–2398 (1994).
14. Sugawara, E. *et al.* Soft magnetic properties of composite-anisotropy CoNbZr/ceramics multilayers (invited). *J. Appl. Phys.* **73,** 5580–5585 (1993).
15. Li, S. *et al.* Quasi magnetic isotropy and microwave performance of FeCoB multilayer laminated by uniaxial anisotropic layers. *J. Appl. Phys.* **115,** 17A310 (2014).
16. Frommberger, M., McCord, J. & Quandt, E. High-frequency properties of FeCoSiB thin films with crossed anisotropy. *IEEE Trans. Magn.* **40,** 2703–2705 (2004).
17. Frommberger, M., McCord, J. & Quandt, E. Crossed anisotropy magnetic cores for integrated inductors. *J. Magn. Magn. Mater.* **290-291,** 1487–1490 (2005).
18. Davies, R. P., Cheng, C., Sturcken, N., Bailey, W. E. & Shepard, K. L. Coupled inductors with crossed anisotropy CoZrTa/SiO_2 multilayer cores. *IEEE Trans. Magn.* **49,** 4009–4012 (2013).
19. Kittel, C. Interpretation of anomalous Larmor frequencies in ferromagnetic resonance experiment. *Phys. Rev.* **71,** 270–271 (1947).
20. Yamaguchi, M., Yabukami, S. & Arai, K. I. A new permeance meter based on both lumped elements /transmission line theories. *IEEE Trans. Magn.* **32,** 4941–4943 (1996).
21. Klemmer, T. J., Ellis, K. A., Chen, L. H., Dover, B. & Jin, S. Ultrahigh frequency permeability of sputtered Fe–Co–B thin films. *J. Appl. Phys.* **87,** 830–833 (2000).
22. Greve, H. *et al.* Nanostructured magnetic Fe–Ni–Co/Teflon multilayers for high-frequency applications in the gigahertz range. *Appl. Phys. Lett.* **89,** 242501 (2008).
23. Ha, N. D., Phan, M. & Kim, C. O. Novel nanostructure and magnetic properties of Co–Fe–Hf–O films. *Nanotechnology* **18,** 155705 (2007).
24. Fan, X. *et al. In situ* fabrication of $Co_{90}Nb_{10}$ soft magnetic thin films with adjustable resonance frequency from 1.3 to 4.9 GHz. *Appl. Phys. Lett.* **92,** 222505 (2008).
25. Li, S., Huang, Z., Duh, J. G. & Yamaguchi, M. Ultrahigh-frequency ferromagnetic properties of FeCoHf films deposited by gradient sputtering. *Appl. Phys. Lett.* **92,** 092501 (2008).
26. Phuoc, N. N. & Ong, C. K. Anomalous temperature dependence of magnetic anisotropy in gradient-composition sputterred thin films. *Adv. Mater.* **25,** 980–984 (2013).
27. Shimada, Y. *et al.* Granular thin films with high RF permeability. *IEEE Trans. Magn.* **39,** 3052–3056 (2003).
28. Ni, W., Kim, J. & Kan, E. C. Permalloy patterning effects on RF inductors. *IEEE Trans. Magn.* **42,** 2827–2829 (2006).
29. Chen, X., Ma, Y. G. & Ong, C. K. Magnetic anisotropy and resonance frequency of patterned soft magnetic strips. *J. Appl. Phys.* **104,** 013921 (2008).
30. Han, X. M. *et al.* Tunable in-plane uniaxial anisotropy and the magnetization reversal mechanism of patterned high-frequency soft magnetic FeTa strips. *J. Phys. D: Appl. Phys.* **46,** 485004 (2013).
31. Viala, B., Inturi, V. R. & Barnard, J. A. Effect of magnetic annealing on the behavior of FeTaN films. *J. Appl. Phys.* **81,** 4498–4500 (1997).
32. Xi, L. *et al.* Influence of magnetic annealing on high-frequency magnetic properties of FeCoNd films. *Mater. Sci. Eng. B* **176,** 1317–1321 (2011).
33. Johnson, F., Um, C. Y., McHenry, M. E. & Garmestani, H. The influence of composition and field annealing on magnetic properties of FeCo-based amorphous and nanocrystalline alloys. *J. Magn. Magn. Mater.* **297,** 93–98 (2006).
34. Prutton, M. Stress and magnetic anisotropy in thin permalloy films. *Nature* **193,** 565–566 (1962).
35. Fu, Y. *et al.* Induced anisotropy in soft magnetic $Fe_{65}Co_{35}$/Co thin films. *Mater. Sci. Eng. B* **133,** 61–65 (2006).
36. Botters, B. *et al.* Stress dependence of ferromagnetic resonance and magnetic anisotropy in a thin NiMnSb film on InP(001). *Appl. Phys. Lett.* **89,** 242505 (2006).
37. Smith, D. O., Cohen, M. S. & Weiss, G. P. Oblique-incidence anisotropy in evaporated Permalloy films. *J. Appl. Phys.* **31,** 1755–1762 (1960).
38. Wang, G. *et al.* Observation of rotatable stripe domain in Permalloy films with oblique sputtering. *J. Appl. Phys.* **112,** 093907 (2012).
39. Chen, Y. *et al.* Designing and Tuning Magnetic Resonance with Exchange Interaction. *Adv. Mater.* **27,** 1351–1355 (2015).
40. Liu, M. *et al.* Voltage-impulse-induced non-volatile ferroelastic switching of ferromagnetic resonance for reconfigurable magnetoelectric microwave devices. *Adv. Mater.* **25,** 4886–4892 (2013).
41. Liu, M. *et al.* Voltage tuning of ferromagnetic resonance with bistable magnetization switching in energy-efficient magnetoelectric composites. *Adv. Mater.* **25,** 1435–1439 (2013).
42. Prosen, R. J., Holmen, J. O. & Gran, B. E. Rotatable anisotropy in thin Permalloy films. *J. Appl. Phys.* **32,** S91–S92 (1961).
43. Fujiwara, H., Sugita, Y. & Saito, N. Mechanism of rotatable anisotropy in thin magnetic films of Ni, Fe, and Ni–Fe. *Appl. Phys. Lett.* **4,** 199–200 (1964).

44. McCord, J., Mattheis, R. & Elefant, D. Dynamic magnetic anisotropy at the onset of exchange bias: the NiFe/IrMn ferromagnet/antiferromagnet system. *Phys. Rev. B* **70,** 094420 (2004).
45. Stiles, M. D. & McMichael, R. D. Model for exchange bias in polycrystalline ferromagnet-antiferromagnet bilayers. *Phys. Rev. B* **59,** 3722–3733 (1999).
46. Chai, G., Phuoc, N. N. & Ong, C. K. Exchange coupling driven omnidirectional rotatable anisotropy in ferrite doped CoFe thin film. *Sci. Rep.* **2,** 832–836 (2012).
47. Gilbert, T. L. A Phenomenological Theory of Damping in Ferromagnetic Materials. *IEEE Trans. Magn.* **40,** 3443–3449 (2004).
48. Ge, S. *et al.* Microstructure and magnetism of FeCo–SiO2 nano-granular films for high frequency application. *J Phys. D: Appl. Phys.* **40,** 3660–3664 (2007).
49. Zhang, Z. *et al.* Optimized soft magnetic properties and high frequency characteristics of obliquely deposited Co–Zr thin films. *J. Phys. D: Appl. Phys.* **43,** 085002 (2010).
50. Wang, Z. *et al.* Fabrication of $Co_{90}Zr_{10}$ thin films with adjustable resonance frequency from 1.8 to 7.1 GHz. *J. Alloy. Compd.* **628,** 236–239 (2015).
51. Smith, D. O. Anisotropy in Permalloy Films. *J. Appl. Phys.* **30,** S264 (1959).
52. Tait, R. N., Smy, T. & Brett, M. J. Structural anisotropy in oblique incidence thin metal films. *J. Vac. Sci. Technol. A* **10,** 1518–1521 (1992).
53. Hoshi, Y., Suzuki, E. & Naoe, M. Uniaxial magnetic anisotropy of iron thin films deposited by oblique incidence of deposition particles. *J. Appl. Phys.* **79,** 4945–4947 (1996).
54. Liu, Y., Chen, L., Tan, C. Y., Liu, H. J. & Ong, C. K. Broadband complex permeability characterization of magnetic thin films using shorted microstrip transmission-line perturbation. *Rev. Sci. Instrum.* **76,** 063911 (2005).

Acknowledgements

This work is supported by the National Basic Research Program of China (No. 2012CB933101), National Natural Science Foundation of China (NSFC) (Nos. 51471080 and 51371093) and the Fundamental Research Funds for the Central Universities (No. lzujbky-2014-40).

Author Contributions

D.X. and G.C. designed this research project, L.P., F.W. and W.W. performed the experiments and analyzed the results. All authors reviewed the manuscript.

Additional Information

Supplementary information accompanies this paper at http://www.nature.com/srep

Competing financial interests: The authors declare no competing financial interests.

How to cite this article: Pan, L. *et al.* In-plane Isotropic Microwave Performance of CoZr Trilayer in GHz Range. *Sci. Rep.* **6**, 21327; doi: 10.1038/srep21327 (2016).